# Proton-Coupled Electron Transfer in Soybean Lipoxygenase

Elizabeth Hatcher, Alexander V. Soudackov, and Sharon Hammes-Schiffer*

*Contribution from the Department of Chemistry, 152 Davey Laboratory,
Pennsylvania State University, University Park, Pennsylvania, 16802*

Received November 14, 2003;  E-mail: shs@chem.psu.edu

***Abstract:*** The proton-coupled electron transfer reaction catalyzed by soybean lipoxygenase-1 is studied with a multistate continuum theory that represents the transferring hydrogen nucleus as a quantum mechanical wave function. The inner-sphere reorganization energy of the iron cofactor is calculated with density functional theory, and the outer-sphere reorganization energy of the protein is calculated with the frequency-resolved cavity model for conformations obtained with docking simulations. Both classical and quantum mechanical treatments of the proton donor−acceptor vibrational motion are presented. The temperature dependence of the calculated rates and kinetic isotope effects is in agreement with the experimental data. The weak temperature dependence of the rates is due to the relatively small free energy barrier arising from a balance between the reorganization energy and the reaction free energy. The unusually high deuterium kinetic isotope effect of 81 is due to the small overlap of the reactant and product proton vibrational wave functions and the dominance of the lowest energy reactant and product vibronic states in the tunneling process. The temperature dependence of the kinetic isotope effect is strongly influenced by the proton donor−acceptor distance with the dominant contribution to the overall rate. This dominant proton donor−acceptor distance is significantly smaller than the equilibrium donor−acceptor distance and is determined by a balance between the larger coupling and the smaller Boltzmann probability as the distance decreases. Thus, the proton donor−acceptor vibrational motion plays a vital role in decreasing the dominant donor−acceptor distance relative to its equilibrium value to facilitate the proton-coupled electron transfer reaction.

## I. Introduction

Lipoxygenases catalyze the oxidation of unsaturated fatty acids and have a wide range of biomedical applications. In mammals, lipoxygenases aid in the production of leukotrienes and lipoxins, which regulate responses in inflammation and immunity.[1] Thus, lipoxygenase inhibitors have been used as drug agents to treat inflammatory diseases such as asthma, atherosclerosis, and psoriasis.[1,2] In addition, lipoxygenase inhibitors have been proposed as promising cancer chemopreventive agents.[3−6] Numerous kinetic studies of lipoxygenases have been carried out using soybean lipoxygenase-1 (SLO)[7] and human lipoxygenase[8] with the substrate linoleic acid.[9] As shown in Figure 1, the pro-*S* hydrogen atom from carbon atom C11 of linoleic acid is transferred to the Fe(III)−OH cofactor, forming
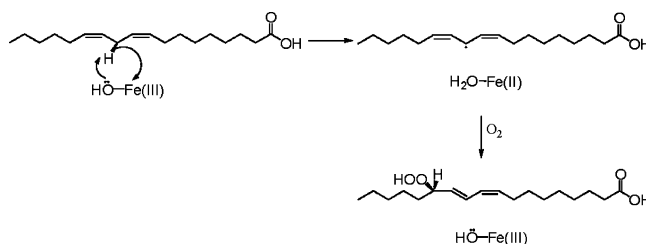


**Figure 1.** Proposed mechanism of soybean lipoxygenase.[7] This article focuses on the first step, which involves the net hydrogen atom transfer from the linoleic acid substrate to the Fe(III)−OH cofactor.

a radical intermediate substrate and Fe(II)−OH$_2$.[7] Subsequent reaction with molecular oxygen eventually leads to hydroperoxyoctadecadienoic acid and Fe(III)−OH.

The hydrogen transfer step in SLO has been investigated with a wide range of experimental and theoretical techniques. Kinetic studies have shown that this step is rate-limiting above 32 °C for SLO.[10] Quantum mechanical calculations indicate that the electron transfers from the $\pi$-system of the linoleic acid to an orbital localized on the Fe(III) center, and the proton transfers from the donor carbon to the oxygen acceptor.[11] Thus, although the reaction involves a net hydrogen atom transfer, the electron and proton are transferred between distinct donors and acceptors. Moreover, analysis of the thermodynamic properties of the single

(1) Samuelsson, B.; Dahlen, S.-E.; Lindgren, J.; Rouzer, C. A.; Serhan, C. N. *Science* **1987**, *237*, 1171−1176.
(2) Holman, T. R.; Zhou, J.; Solomon, E. L. *J. Am. Chem. Soc.* **1998**, *120*, 12564−12572.
(3) Steele, V. E.; Holmes, C. A.; Hawk, E. T.; Kopelovich, L.; Lubet, R. A.; Crowell, J. A.; Sigman, C. C.; Kelloff, G. J. *Cancer Epidemiol., Biomarkers Prev.* **1999**, *8*, 467−483.
(4) Rioux, N.; Castonguay, A. *Carcinogenesis* **1998**, *19*, 1393−1400.
(5) Nie, D.; Hillman, G. G.; Geddes, T.; Tang, K.; Pierson, C.; Grignon, D. J.; Honn, K. V. *Cancer Res.* **1998**, *58*, 4047−4051.
(6) Ghosh, J.; Myers, C. E. *Proc. Natl. Acad. Sci. U.S.A.* **1998**, *95*, 13182−13187.
(7) Rickert, K. W.; Klinman, J. P. *Biochemistry* **1999**, *38*, 12218−12228.
(8) Lewis, E. R.; Johansen, E.; Holman, T. R. *J. Am. Chem. Soc.* **1999**, *121*, 1395−1396.
(9) Although the natural substrate for human lipoxygenase is arachidonic acid, it also reacts with linoleic acid.[8]

(10) Glickman, M. H.; Klinman, J. P. *Biochemistry* **1995**, *34*, 14077−14092.
(11) Lehnert, N.; Solomon, E. L. *J. Biol. Inorg. Chem.* **2003**, *8*, 294−305.

proton transfer (PT) and electron transfer (ET) reactions, as well as the concerted proton-coupled electron transfer (PCET) mechanism, indicates that the single PT and ET reactions are significantly endothermic, whereas the PCET reaction is exothermic.[11,12] On the basis of these analyses, the proposed mechanism for this reaction is a PCET in which the electron and proton transfer simultaneously between different donors and acceptors.

The deuterium kinetic isotope effect (KIE) on the catalytic rate for SLO has been measured to be as high as 81 at room temperature.[7,12–15] Large KIEs have also been measured for human lipoxygenase.[8] The temperature dependence of the KIEs has been analyzed in terms of various tunneling models.[7,13] These theoretical studies suggest that hydrogen tunneling plays a central role in this reaction. The importance of gating, which is defined in terms of vibrational modes that modulate the hydrogen transfer distance, has also been discussed.[12] In addition, a number of mutants of SLO have been studied experimentally and theoretically.[12,16]
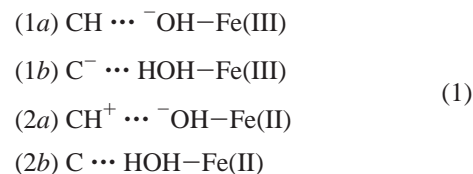
In this article, we investigate the PCET reaction in SLO with a multistate continuum theory.[17–19] In this theoretical formulation, the PCET reaction is described in terms of the four charge transfer states involving the proton and the electron, and the transferring hydrogen nucleus is represented by a quantum mechanical wave function. The conformations of the linoleic acid bound to SLO are investigated with docking calculations. The reorganization energy of the iron complex is examined with density functional theory (DFT) methods, and the reorganization energy of the protein environment is calculated within the dielectric continuum approximation using the frequency-resolved cavity model.[20,21] The multistate continuum theory calculations reproduce the experimentally observed temperature dependence of the rates and KIEs for a range of physically reasonable parameter values. An analysis of the results elucidates the detailed mechanism of the PCET reaction and provides an explanation for the unusually large magnitude and observed temperature dependence of the KIE.

## II. Theory

PCET reactions have been studied with a variety of theoretical methods.[17–19,22–24] The theoretical formulation used to describe ET and PCET reactions in this article is based primarily on the recently developed multistate continuum theory.[17–19] In this formulation, the solute is described by a multistate valence bond model, the transferring hydrogen nucleus is treated quantum

mechanically, and the solvent is represented as a dielectric continuum. This theory may be used to calculate the free-energy surfaces for PCET as functions of two collective solvent coordinates corresponding to PT and ET, respectively. The multistate continuum theory also provides rate expressions for PCET reactions.[18]

The PCET reaction catalyzed by lipoxygenase may be described in terms of the following four electronic diabatic states:

$$
\begin{aligned}
&(1a)\ \text{CH} \cdots {}^-\text{OH}-\text{Fe(III)} \\
&(1b)\ \text{C}^- \cdots \text{HOH}-\text{Fe(III)} \\
&(2a)\ \text{CH}^+ \cdots {}^-\text{OH}-\text{Fe(II)} \\
&(2b)\ \text{C} \cdots \text{HOH}-\text{Fe(II)}
\end{aligned}
\tag{1}
$$

where 1 and 2 denote the ET state and *a* and *b* denote the PT state. The proton is transferred from the C11 carbon atom of the linoleic acid to the oxygen atom of the Fe-bound OH ligand, and the electron is transferred from the $\pi$-system of the linoleic acid to the iron. Within this notation, $1a \rightarrow 1b$ represents PT, $1a \rightarrow 2a$ represents ET, and $1a \rightarrow 2b$ represents EPT (where both the proton and the electron are transferred).

As shown in ref 17, the free energy surfaces for PCET reactions may be calculated as functions of two collective solvent coordinates $z_p$ and $z_e$, corresponding to PT and ET, respectively. For the systems studied in this article, the PT reaction is electronically adiabatic, while the ET/EPT reactions are assumed to be electronically nonadiabatic.[25] In this case, the ET diabatic free energy surfaces corresponding to ET states 1 and 2 are calculated as mixtures of the *a* and *b* PT states. The reactants (I) are mixtures of the 1*a* and 1*b* states, and the products (II) are mixtures of the 2*a* and 2*b* states. The proton vibrational states are calculated for both the reactant (I) and product (II) ET diabatic surfaces, resulting in two sets of two-dimensional vibronic free energy surfaces that may be approximated as paraboloids. In this theoretical formulation, the PCET reaction is described in terms of nonadiabatic transitions from the reactant (I) to the product (II) ET diabatic surfaces. Thus, the ET diabatic states I and II, respectively, may be viewed as the reactant and product PCET states. Note that EPT refers to a transition between pure diabatic states 1*a* and 2*b*, whereas PCET refers to a transition between mixed ET diabatic states I (1*a*/1*b*) and II (2*a*/2*b*). For the system studied in this article, the lowest energy PCET reactant state I is predominantly 1*a*, and the lowest energy PCET product state II is predominantly 2*b*.

The unimolecular rate expression derived in ref 18 for PCET is

$$
k^{\text{PCET}} = \frac{2\pi}{\hbar} \sum_\mu P_{\text{I}\mu} \sum_\nu |V_{\mu\nu}|^2 (4\pi\lambda_{\mu\nu}k_{\text{B}}T)^{-1/2} \exp\left(\frac{-\Delta G_{\mu\nu}^\dagger}{k_{\text{B}}T}\right)
\tag{2}
$$

where $\sum_\mu$ and $\sum_\nu$ indicate summations over vibrational states

(12) Knapp, M. J.; Rickert, K. W.; Klinman, J. P. *J. Am. Chem. Soc.* **2002**, *124*, 3865−3874.
(13) Jonsson, T.; Glickman, M. H.; Sun, S.; Klinman, J. P. *J. Am. Chem. Soc.* **1996**, *118*, 10319−10320.
(14) Glickman, M. H.; Wiseman, J. S.; Klinman, J. P. *J. Am. Chem. Soc.* **1994**, *116*, 793−794.
(15) Hwang, C.-C.; Grissom, C. B. *J. Am. Chem. Soc.* **1994**, *116*, 795−796.
(16) Knapp, M. J.; Seebeck, F. P.; Klinman, J. P. *J. Am. Chem. Soc.* **2001**, *123*, 2931−2932.
(17) Soudackov, A.; Hammes-Schiffer, S. *J. Chem. Phys.* **1999**, *111*, 4672−4687.
(18) Soudackov, A.; Hammes-Schiffer, S. *J. Chem. Phys.* **2000**, *113*, 2385−2396.
(19) Hammes-Schiffer, S. *Acc. Chem. Res.* **2001**, *34*, 273−281.
(20) Basilevsky, M. V.; Rostov, I. V.; Newton, M. D. *Chem. Phys.* **1998**, *232*, 189−199.
(21) Newton, M. D.; Basilevsky, M. V.; Rostov, I. V. *Chem. Phys.* **1998**, *232*, 201−210.
(22) Cukier, R. I. *J. Phys. Chem.* **1996**, *100*, 15428−15443.
(23) Cukier, R. I.; Nocera, D. G. *Annu. Rev. Phys. Chem.* **1998**, *49*, 337−369.
(24) Mayer, J. M.; Hrovat, D. A.; Thomas, J. L.; Borden, W. T. *J. Am. Chem. Soc.* **2002**, *124*, 11142−11147.

(25) Here electronically adiabatic refers to reactions occurring in the electronic ground state, and electronically nonadiabatic refers to reactions involving excited electronic states. An ET reaction is nonadiabatic if the coupling between the electron transfer states is much less than the thermal energy. Even if the ET reaction were adiabatic, the overall PCET reaction for the system studied in this article is expected to be nonadiabatic (i.e., the overall coupling $V_{\mu\nu}$ is much less than the thermal energy) due to the small overlap between the dominant reactant and product hydrogen vibrational wave functions.

associated with ET states 1 and 2, respectively, $P_{I\mu}$ is the Boltzmann probability for state $I\mu$, and $\Delta G^{\dagger}_{\mu\nu}$ is the free energy barrier defined as

$$\Delta G^{\dagger}_{\mu\nu} = \frac{(\Delta G^{o}_{\mu\nu} + \lambda_{\mu\nu})^2}{4\lambda_{\mu\nu}} \qquad (3)$$

In this expression, the free energy of reaction is defined as

$$\Delta G^{o}_{\mu\nu} = \epsilon^{II}_{\nu}(\bar{z}^{II\nu}_{p}, \bar{z}^{II\nu}_{e}) - \epsilon^{I}_{\mu}(\bar{z}^{I\mu}_{p}, \bar{z}^{I\mu}_{e}) \qquad (4)$$

where $(\bar{z}^{I\mu}_{p}, \bar{z}^{I\mu}_{e})$ and $(\bar{z}^{II\nu}_{p}, \bar{z}^{II\nu}_{e})$ are the solvent coordinates for the minima of the ET diabatic free energy surfaces $\epsilon^{I}_{\mu}(z_p, z_e)$ and $\epsilon^{II}_{\nu}(z_p, z_e)$, respectively. Moreover, in the high-temperature approximation for uncoupled solute modes, the total reorganization energy is expressed as the sum of the outer-sphere (solvent) and inner-sphere (solute) contributions:

$$\lambda_{\mu\nu} = (\lambda_o)_{\mu\nu} + \lambda_{in} \qquad (5)$$

where the outer-sphere reorganization energy is defined as

$$\begin{aligned}(\lambda_o)_{\mu\nu} &= \epsilon^{I}_{\mu}(\bar{z}^{II\nu}_{p}, \bar{z}^{II\nu}_{e}) - \epsilon^{I}_{\mu}(\bar{z}^{I\mu}_{p}, \bar{z}^{I\mu}_{e}) \\ &= \epsilon^{II}_{\nu}(\bar{z}^{I\mu}_{p}, \bar{z}^{I\mu}_{e}) - \epsilon^{II}_{\nu}(\bar{z}^{II\nu}_{p}, \bar{z}^{II\nu}_{e})\end{aligned} \qquad (6)$$

The inner-sphere reorganization energy $\lambda_{in}$ will be discussed below. The coupling $V_{\mu\nu}$ in the PCET rate expression is defined as

$$V_{\mu\nu} = \langle \phi^{I}_{\mu} | V(r_p, z^{\dagger}_p) | \phi^{II}_{\nu} \rangle_p \qquad (7)$$

where the subscript of the angular brackets indicates integration over the proton coordinate $r_p$, $z^{\dagger}_p$ is the value of $z_p$ in the intersection region, and $\phi^{I}_{\mu}$ and $\phi^{II}_{\nu}$ are the proton vibrational wave functions for the reactant and product ET diabatic states, respectively.

Recently, the multistate continuum theory has been extended to include the motion between the proton donor and acceptor.[26] For the classical treatment of the donor–acceptor vibrational mode $R$, we use the following expression to calculate the total rate:

$$\begin{aligned}k^{PCET}_{tot} &= \frac{2\pi}{\hbar} \int_0^\infty dR \sum_\mu P_{I\mu}(R) \sum_\nu |V_{\mu\nu}(R)|^2 [4\pi\lambda_{\mu\nu}(R)k_BT]^{-1/2} \\ &\times \exp\left[\frac{-\Delta G^{\dagger}_{\mu\nu}(R)}{k_BT}\right]\end{aligned} \qquad (8)$$

where all of the quantities are defined analogously as for eq 2 and are evaluated at a particular proton donor–acceptor distance $R$. (Note that this thermal averaging is based on the assumption that a Boltzmann distribution is maintained for the proton donor–acceptor vibrational mode.) Thus, the two-dimensional vibronic free energy surfaces and the corresponding PCET rates are calculated for a series of proton donor–acceptor distances along a grid, and the integral in eq 8 is evaluated numerically. Note that the normalization constant for the Boltzmann probability $P_{I\mu}(R)$ is calculated by integrating over $R$ as well as

summing over reactant vibronic states $\mu$. For the quantum mechanical treatment of the donor–acceptor vibrational mode $R$, we use the general form of the rate expression given in eq 2 in conjunction with two-dimensional vibrational wave functions that depend on the hydrogen coordinate $r_p$ and the proton donor–acceptor distance $R$. The two-dimensional vibrational wavefunctions are calculated for both the reactant (I) and product (II) ET diabatic surfaces, resulting in two sets of vibronic surfaces that are used to determine the input quantities for eq 2.

The inner-sphere reorganization energy for the PCET reaction due to the Fe–ligand bonds is approximated as[27]

$$\lambda_{in} = \sum_j \frac{f^r_j f^p_j}{f^r_j + f^p_j}(\Delta q_j)^2 \qquad (9)$$

where the summation is over the six Fe–ligand modes (assumed to be harmonic), $f^r_j$ and $f^p_j$ are the equilibrium force constants of the $j$th mode in the reactant and product, respectively, and $\Delta q_j$ is the difference in the reactant and product equilibrium bond lengths for the $j$th mode. For the system studied in this article, the inner-sphere reorganization energy is calculated between the diabatic states $1a$ and $2b$ because these diabatic states are dominant in the reactant and product PCET states.

## III. Calculation of Input Quantities

Within the framework of this theoretical formulation,[17–19] the calculation of the rates and KIEs requires the inner-sphere reorganization energy, the solvent reorganization energy matrix elements, and the gas-phase valence bond matrix elements. For the classical treatment of the donor–acceptor mode, the calculation of the rates involves the following three steps. In the first step of the procedure, the two-dimensional free energy surfaces $\epsilon^{I}_{\mu}(z_p, z_e)$ and $\epsilon^{II}_{\nu}(z_p, z_e)$ corresponding to the solvated reactant and product vibronic states are calculated for a series of proton donor–acceptor distances $R$ along a grid. These surfaces are calculated from the gas-phase valence bond matrix elements and the solvent reorganization energy matrix elements using the analytical expressions given in ref 17. In the second step, the free energy difference $\Delta G^{o}_{\mu\nu}$ and the solvent reorganization energy $(\lambda_o)_{\mu\nu}$ are determined for each pair of vibronic states using eqs 4 and 6, respectively, at each grid point for $R$. The coupling $V_{\mu\nu}$ for each pair of vibronic states is determined from the associated vibrational wave functions and the off-diagonal gas-phase valence bond matrix elements using eq 7. In the third step, these quantities and the inner-sphere reorganization energy are used to calculate the total PCET rate with eq 8 (or eq 2 for a fixed value of $R$).

Thus, this theoretical formulation requires three types of input quantities. The inner-sphere (solute) reorganization energy $\lambda_{in}$ may be calculated from the equilibrium force constants and bond lengths. In this article, the outer-sphere (solvent) reorganization energy matrix elements are calculated with an electrostatic dielectric continuum model. In practice, the gas-phase valence bond matrix elements are represented by molecular mechanical terms fit to electronic structure calculations or experimental data.[28]

(26) Soudackov, A. V.; Hatcher, E.; Hammes-Schiffer, S., to be submitted for publication.

(27) Zhou, Z.; Khan, S. U. M. *J. Phys. Chem.* **1989**, *93*, 5292–5295.

(28) Warshel, A. *Computer Modeling of Chemical Reactions in Enzymes and Solutions*; John Wiley & Sons: New York, 1991.
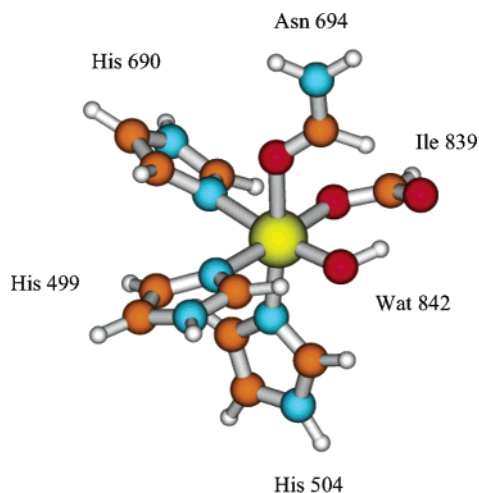
**Figure 2.** Model iron complex used for the DFT B3LYP calculations with the geometry optimized for the Fe(III)−OH state.

**Table 1.** DFT B3LYP Results for the Fe−Ligand Distances for the Four Diabatic States of the Model System in Figure 2

|  | Fe(III)–OH | Fe(III)–OH$_2$ | Fe(II)–OH | Fe(II)–OH$_2$ |
|---|---|---|---|---|
| Fe−His499 N$\epsilon$2 | 2.16 | 2.11 | 2.24 | 2.18 |
| Fe−His504 N$\epsilon$2 | 2.14 | 2.11 | 2.21 | 2.19 |
| Fe−His690 N$\epsilon$2 | 2.18 | 2.08 | 2.27 | 2.14 |
| Fe−Asn694 O$\delta$1 | 2.18 | 2.05 | 2.30 | 2.22 |
| Fe−Ile839 O1 | 2.05 | 2.02 | 2.22 | 2.23 |
| Fe−Wat842 O | 1.86 | 2.13 | 1.97 | 2.17 |

**Inner-Sphere Reorganization Energy.** The inner-sphere reorganization energy due to the Fe−ligand bonds was determined from eq 9. The force constants were obtained from experimental measurements on model compounds.[27] Specifically, the force constants for [Fe(NH$_3$)$_6$]$^{2+}$ and [Fe(NH$_3$)$_6$]$^{3+}$ of 148 and 232 kcal mol$^{-1}$ Å$^{-2}$ are used for the three histidines (His499, His504, His690) and the force constants for [Fe(H$_2$O)$_6$]$^{2+}$, [Fe(H$_2$O)$_6$]$^{3+}$ of 230 and 366 kcal mol$^{-1}$ Å$^{-2}$ are used for Asn694, Ile839, and Wat842. The values for $\Delta q_j$ are determined from geometry optimizations with density functional theory at the B3LYP/LanL2DZ level[29−32] for the model system depicted in Figure 2. All electronic structure calculations in this article were performed with Gaussian98.[33] In this model, the amino acids are represented by the relevant fragments: histidines by imidazole rings, asparagine by a formamide molecule, and isoleucine by a formic anion. We performed optimizations for Fe(III) and Fe(II) complexes with both a water and a hydroxide ligand. Table 1 gives the Fe−ligand bond lengths for the four different complexes. These results are consistent with previous
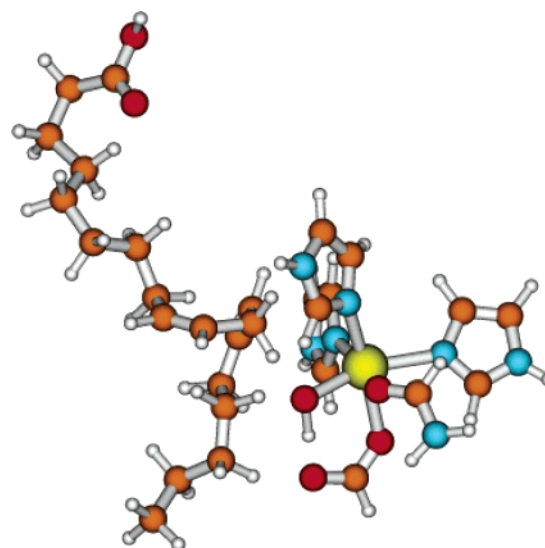
(29) Lee, C.; Yang, W.; Parr, P. G. *Phys. Rev. B* **1988**, *45*, 785.
(30) Becke, A. D. *J. Chem. Phys.* **1993**, *98*, 5648.
(31) Dunning, J., T. H.; Hay, P. J. *Modern Theoretical Chemistry*; Plenum: New York, 1976; Vol. 3.
(32) Hay, P. J.; Wadt, W. R. *J. Chem. Phys.* **1984**, *82*, 270.
(33) Frisch, M. J.; Trucks, G. W.; Schlegel, H. B.; Scuseria, G. E.; Robb, M. A.; Cheeseman, J. R.; Zakrzewski, V. G.; Montgomery, J. A., Jr.; Stratmann, R. E.; Burant, J. C.; Dapprich, S.; Millam, J. M.; Daniels, A. D.; Kudin, K. N.; Strain, M. C.; Farkas, O.; Tomasi, J.; Barone, V.; Cossi, M.; Cammi, R.; Mennucci, B.; Pomelli, C.; Adamo, C.; Clifford, S.; Ochterski, J.; Petersson, G. A.; Ayala, P. Y.; Cui, Q.; Morokuma, K.; Malick, D. K.; Rabuck, A. D.; Raghavachari, K.; Foresman, J. B.; Cioslowski, J.; Ortiz, J. V.; Stefanov, B. B.; Liu, G.; Liashenko, A.; Piskorz, P.; Komaromi, I.; Gomperts, R.; Martin, R. L.; Fox, D. J.; Keith, T.; Al-Laham, M. A.; Peng, C. Y.; Nanayakkara, A.; Gonzalez, C.; Challacombe, M.; Gill, P. M. W.; Johnson, B. G.; Chen, W.; Wong, M. W.; Andres, J. L.; Head-Gordon, M.; Replogle, E. S.; Pople, J. A. *Gaussian 98*, revision A.7; Gaussian, Inc.: Pittsburgh, PA, 1998.

**Figure 3.** Conformation of linoleic acid and the iron cofactor obtained from docking calculations that included the entire SLO protein.

calculations on the Fe(III)OH and Fe(II)OH$_2$ model complexes.[34] The calculated Fe−ligand distances were used to estimate the inner-sphere reorganization energy to be 19 kcal/mol.

**Outer-Sphere Reorganization Energies.** The solvent reorganization energies are calculated with the frequency-resolved cavity model (FRCM) developed by Newton, Rostov, and Basilevsky.[20,21] This approach allows for distinct effective solute cavities pertaining to the optical and inertial solvent response. The cavities are formed from spheres centered on all of the atoms. The two effective radii for the solute atoms are defined as $r_\infty = \kappa r_{vdW}$ and $r_{in} = r_\infty + \delta$, where $r_{vdW}$ is the van der Waals radius, $\kappa$ is a universal scaling factor, and $\delta$ is a constant specific to the particular solvent. In our calculations, $\kappa = 0.9$ and $\delta = 0.9$, as determined for cations in water.[21] The static dielectric constant for the protein was chosen to be $\epsilon_o = 4.0$,[35] and the optical dielectric constant was chosen to be $\epsilon_\infty = 1.78$, as for water. The solvation properties are calculated with the model shown in Figure 3, which includes all atoms of the linoleic acid and an iron complex. The charge density of each diabatic (i.e., valence bond) state is defined by assigning appropriate partial charges to all atoms. The reorganization energy matrix element between diabatic states $i$ and $j$ is determined by calculating the interaction of the charge density of state $i$ with the dielectric continuum solvent response to the charge density of state $j$.

The atomic coordinates utilized for the FRCM calculations were obtained from docking calculations on linoleic acid and SLO. We used the AutoDock 3.0.5 program[36] to perform these docking calculations. In these calculations, the protein (including the Fe(III)−OH cofactor) is fixed at the crystal structure coordinates obtained from the Brookhaven Protein Data Bank (pdb code 1F8N).[37] During the docking procedure, the linoleic acid is flexible within a grid of dimensions 30 × 15 × 15 Å spanning the cavity region. We generated 1000 different

(34) Borowski, T.; Krol, M.; Chruszcz, M.; Broclawik, E. *J. Phys. Chem. B* **2001**, *105*, 12212−12220.
(35) Olson, M. A.; Reinke, L. T. *Proteins: Struct., Funct., Genet.* **2000**, *38*, 115−119.
(36) Morris, G. M.; Goodsell, D. S.; Halliday, R. S.; Huey, R.; Hart, W. E.; Belew, R. K.; Olson, A. J. *J. Comput. Chem.* **1998**, *19*, 1639−1662.
(37) Tomchick, D. R.; Phan, P.; Cymbrowski, M.; Minor, W.; Holman, T. R. *Biochemistry* **2001**, *40*, 7509−7517.

conformations. We chose several suitable conformations on the basis of the C−O distance and the CHO angle. One of the suitable conformations is depicted in Figure 3. This conformation has a C−O distance of 2.83 Å and a CHO angle of 152°, and the carboxylate group of the linoleic acid is oriented opposite to the isoleucine ligand as found in the purple bacteria.[38] We calculated the solvent reorganization energy matrix elements for this conformation and for two other conformations with C−O distances of 3.0 and 3.2 Å, respectively. We found that the solvent reorganization energies are not sensitive to the specific choice of conformation.

The atomic charges for the diabatic states used for the FRCM calculations in this article were designated as follows. The iron atom was assigned a charge of +2 or +3, corresponding to the appropriate oxidation state. The atomic charges on the His499, His504, His690, Asn694, and Ile839 ligands were obtained with the CHELPG method[39] based on DFT B3LYP/6-31G** calculations for each individual ligand with the crystal structure coordinates. The atomic charges for the water ligand were obtained with the CHELPG method based on DFT B3LYP/6-31G** calculations for an optimized isolated water molecule. The atomic charges for the hydroxide ligand were determined by assigning the same charge (+0.36) for the hydrogen as determined for the water ligand and assigning the remainder of the −1 charge to the oxygen atom. The atomic charges on the linoleic acid were obtained by applying the CHELPG method with DFT B3LYP/6-31G** for the conformation determined from the docking calculations. The atomic charge for the transferring hydrogen was assigned +0.36 for diabatic states 1*a* and 2*a*, and the atomic charge for C11 was adjusted to obtain the correct overall charge for each of the four diabatic states. Note that the solvent quantities are approximated to be independent of the proton donor−acceptor distance $R$ within the relevant range.

**Gas-Phase Valence Bond Matrix Elements.** The gas-phase valence bond matrix elements for the PCET reaction are based on a linear, five-site model:

$$\pi_D - C_D - H - O_A - Fe_A$$

where the D and A subscripts denote donor and acceptor, respectively. The proton is transferred from the carbon atom (C_D) of the linoleic acid to the oxygen atom (O_A) of the Fe-bound OH ligand. The electron is transferred from the π-system of the linoleic acid ($\pi_D$) to the iron (Fe_A). The gas-phase valence bond matrix elements are represented by molecular mechanical terms fit to electronic structure calculations and experimental data. We emphasize that this five-site model is used only to provide molecular mechanical functional forms for the gas-phase matrix elements. The carbon, hydrogen, oxygen, and iron atoms are not linear in the conformation obtained from the docking procedure, but the linear model provides a qualitatively reasonable potential for fitting to experimental data. As described above, all atoms of the complex are included in the conformations obtained from the docking procedure for the calculation of solvation properties.

The diagonal matrix elements of the gas-phase Hamiltonian are expressed as

$$(h_o)_{1a,1a} = U_a^{LEPS} + U_{\pi C}^{harm} + U_{FeO}^{harm}$$

$$(h_o)_{1b,1b} = U_b^{LEPS} + U_{\pi C}^{harm} + U_{FeO}^{harm} + \Delta E_{1b}$$

$$(h_o)_{2a,2a} = U_a^{LEPS} + U_{\pi C}^{harm} + U_{FeO}^{harm} + \Delta E_{2a}$$

$$(h_o)_{2b,2b} = U_b^{LEPS} + U_{\pi C}^{harm} + U_{FeO}^{harm} + \Delta E_{2b}$$

$$(10)$$

These diagonal terms represent the potential energy for the unperturbed diabatic states. Note that the positions of the $\pi_D$ and Fe_A sites are fixed, and these matrix elements depend on the positions of the C_D, H, and O_A sites. The proton-transfer interface C_DHO_A is described by a LEPS potential:[40−42]

$$U_a^{LEPS} = Q_{CH} + Q_{OH} + Q_{CO} - \frac{1}{2}(J_{CO} + J_{OH}) + J_{CH}$$

$$U_b^{LEPS} = Q_{CH} + Q_{OH} + Q_{CO} - \frac{1}{2}(J_{CO} + J_{CH}) + J_{OH}$$

$$(11)$$

where the Coulombic and exchange terms are

$$Q_{XY} = \frac{E_{XY}^1(1 + k_{XY}) + E_{XY}^3(1 - k_{XY})}{2(1 + k_{XY})}$$

$$J_{XY} = \frac{E_{XY}^1(1 + k_{XY}) - E_{XY}^3(1 - k_{XY})}{2(1 + k_{XY})}$$

$$(12)$$

and the Morse and anti-Morse potentials are

$$E_{XY}^1 = D_{XY}[\exp(-2\beta_{XY}(R_{XY}-R_{XY}^\circ)) - 2\exp(-\beta_{XY}(R_{XY}-R_{XY}^\circ))]$$

$$E_{XY}^3 = \frac{1}{2}D_{XY}[\exp(-2\beta_{XY}(R_{XY}-R_{XY}^\circ)) + 2\exp(-\beta_{XY}(R_{XY}-R_{XY}^\circ))]$$

$$(13)$$

For simplicity, the empirical Sato parameter $k_{XY}$ was set to 0.5 for all pairs of atoms, similar to the value used previously.[41] The values for $D_{CH}$ and $D_{OH}$ were determined to be 77 and 82 kcal/mol on the basis of the bond dissociation energies discussed in the Appendix. The values for $\beta_{CH}$ and $\beta_{OH}$ were determined to be 2.068 and 2.442 Å$^{-1}$ to reproduce the typical experimentally measured C−H and O−H frequencies of 2900 and 3500 cm$^{-1}$. The values for $R_{CH}^\circ$ and $R_{OH}^\circ$ were determined to be 1.09 and 0.96 Å from typical experimentally measured bond lengths.[28] In the first model studied, the C−O Morse parameters were chosen as follows: $R_{CO}^\circ = 2.83$ Å, the distance in a conformation obtained from docking; $D_{CO} = 8$ kcal/mol, as used in related LEPS potentials;[41] and $\beta_{CO} = 2.5$ Å$^{-1}$, corresponding to a Morse frequency of 415 cm$^{-1}$ for a reduced mass of 6.86 g/mol, to be consistent with the harmonic frequencies of the Fe−O and the carbon atom C11 motions discussed below. In the Results and Discussion section, we discuss the dependence of the results on the C−O Morse parameters $R_{CO}^\circ$ and $\beta_{CO}$ and present the results for an alternative model in which $R_{CO}^\circ = 3.0$ Å and $\beta_{CO} = 1.8$ Å$^{-1}$.

(38) Skrzypczak-Jankun, E.; Bross, R. A.; Carroll, R. T.; Dunham, W. R.; Funk, J. M. O. *J. Am. Chem. Soc.* **2001**, *123*, 10814−10820.
(39) Breneman, C. M.; Wiberg, K. B. *J. Comput. Chem.* **1990**, *11*, 361.
(40) Kuntz, P. J.; Nemeth, E. M.; Polanyi, J. C.; Rosner, S. D.; Young, C. E. *J. Chem. Phys.* **1966**, *44*, 1168−1184.
(41) Kim, Y.; Truhlar, D. G.; Kreevoy, M. M. *J. Am. Chem. Soc.* **1991**, *113*, 7837−7847.
(42) Basilevsky, M. V.; Soudackov, A. V.; Vener, M. V. *Chem. Phys.* **1995**, *200*, 87−106.

The harmonic terms are included in eq 10 to confine the carbon and oxygen atoms between the electron donor and acceptor in a physically reasonable manner. In the first model studied, the force constant for $U_{FeO}^{harm}$ was chosen to be 366 kcal mol$^{-1}$ Å$^{-2}$, corresponding to the experimentally measured value for $[Fe(H_2O)_6]^{3+}$.[27] The equilibrium distance for $U_{FeO}^{harm}$ was chosen to be the value determined from the DFT B3LYP calculations for the Fe(III)–OH state, as given in Table 1. The force constant of 117 kcal mol$^{-1}$ Å$^{-2}$ for $U_{\pi C}^{harm}$ was determined from a DFT B3LYP/6-31G** frequency calculation on an optimized structure for linoleic acid, where the scaling factor[43] of 0.96 was applied to the frequency (339 cm$^{-1}$) of the mode representing the relevant vibrational motion of carbon atom C11. The equilibrium distance for $U_{\pi C}^{harm}$ was chosen to be 1.0 Å. On the basis of the equilibrium distances, the $\pi_D$–Fe$_A$ distance was fixed at 5.69 Å for all diabatic states. Note that the frequency of the C–O vibrational motion is determined mainly by these harmonic frequencies in this model. In the alternative model mentioned above, the force constants for $U_{FeO}^{harm}$ and $U_{\pi C}^{harm}$ were chosen to be 100 and 25 kcal mol$^{-1}$ Å$^{-2}$, respectively, and the frequency of the C–O vibrational motion was determined mainly by the Morse parameter $\beta_{CO}$.

The constants $\Delta E_{1b}$, $\Delta E_{2a}$, and $\Delta E_{2b}$ are fit to reproduce the experimentally determined driving forces (i.e., reaction free energies) for PT, ET, and PCET, respectively. As shown in the Appendix, the resulting reaction free energies are estimated to be:

$$\Delta G_{1a \to 1b}^{oPT} = 32 \text{ kcal/mol}$$

$$\Delta G_{1a \to 2a}^{oET} = 43 \text{ kcal/mol} \qquad (14)$$

$$\Delta G_{1a \to 2b}^{oEPT} = -5.4 \text{ kcal/mol}$$

The parametrized constants $\Delta E_{1b}$, $\Delta E_{2a}$, and $\Delta E_{2b}$ are 36.07, 37.26, and $-20.42$ kcal/mol, respectively.

In this article, the couplings are of the form

$$(h_o)_{1a,1b} = (h_o)_{2a,2b} = -V^{PT} \exp(-\alpha(R_{CO} - R_{CO}^o))$$

$$(h_o)_{1a,2a} = (h_o)_{1b,2b} = V^{ET} \qquad (15)$$

$$(h_o)_{1a,2b} = (h_o)_{1b,2a} = V^{ET}\sigma$$

where the overlap integral $\sigma = 0.5$, as in the standard two-state LEPS model for triatomic collinear systems.[44] The exponential factor $\alpha = 1$ Å$^{-1}$ was chosen to reproduce the $R_{CO}$ dependence of the LEPS off-diagonal term for larger C–O distances:

$$(h_o)_{1a,1b} = (h_o)_{2a,2b}$$

$$\approx \frac{1}{2}(Q_{CH} + Q_{OH} + Q_{CO}) - J_{CO} + \frac{1}{2}(J_{CH} + J_{OH})$$

$$(16)$$

The coupling $V^{ET} = 0.019$ kcal/mol was determined by fitting to the experimental rate for the PCET reaction at $T = 303$ K. The coupling $V^{PT} = 19.5$ kcal/mol was chosen to be similar in magnitude to the couplings used in other related EVB models

(43) Scott, A. P.; Radom, L. *J. Phys. Chem.* **1996**, *100*, 16502–16513.
(44) Glasstone, S.; Laidler, K. J.; Eyring, H. *The Theory of Rate Processes*; McGraw-Hill: New York, 1941.
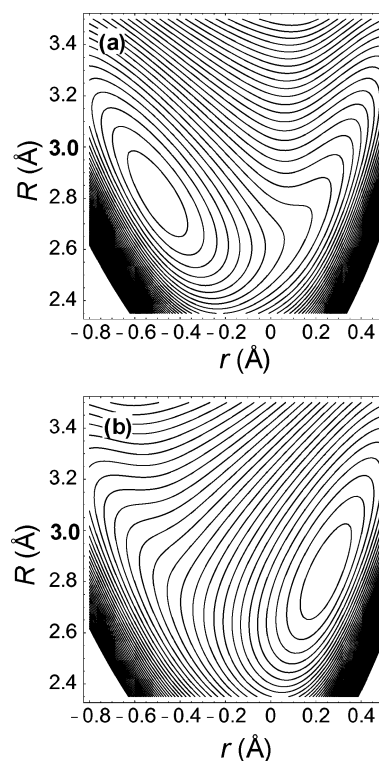
**Figure 4.** Gas-phase EVB potential energy surface as a function of the proton coordinate $r$ and the proton donor–acceptor distance $R$ for (a) ET state 1, which is a mixture of diabatic states 1*a* and 1*b*, and (b) ET state 2, which is a mixture of diabatic states 2*a* and 2*b*.

and was refined to fit the experimental KIE for the PCET reaction at $T = 303$ K.

We emphasize that the gas-phase potential energy surface for each ET diabatic state is a mixture of the PT diabatic states. Specifically, the gas-phase potential energy surface for ET diabatic state 1 is a mixture of the diagonal terms 1*a* and 1*b* given in eq 10, where the degree of mixing is determined by the off-diagonal terms. Moreover, each diabatic state is a combination of LEPS potentials and additional harmonic terms. Thus, typically the equilibrium bond lengths and frequencies for the overall gas-phase potential energy surface are different from the corresponding input parameters for the Morse potentials. The gas-phase potential energy surfaces are depicted in Figure 4.

## IV. Results and Discussion

**Reorganization Energies.** The inner-sphere reorganization energy due to the Fe–ligand bonds was calculated from eq 9, where the force constants were obtained from experimental data and the bond length changes were determined from density functional theory calculations on model compounds. The resulting inner-sphere reorganization energy is 19.1 kcal/mol. As indicated in Table 1, the dominant contribution to this inner-sphere reorganization energy arises from the difference in the Fe(III)–OH and the Fe(II)–OH$_2$ bond lengths.[45,46] Note that this calculation provides only an estimate of the total inner-sphere reorganization energy. The inner-sphere reorganization

(45) This contribution is significantly larger than an estimate based on the inner-sphere reorganization energy[46] for the oxidation of Fe(II)(H$_2$O)$_6$ to Fe(III)(H$_2$O)$_6$ because the ligand is changing from OH to OH$_2$ during the PCET reaction.
(46) Bu, Y.; Liu, S.; Song, X. *Chem. Phys. Lett.* **1994**, *227*, 121–125.

energy due to the Fe−ligand bonds is expected to be somewhat smaller in the protein than in the gas phase. Moreover, the reorganization of the linoleic acid substrate may also contribute to the total inner-sphere reorganization energy. At the end of this section, we discuss the dependence of the results on the inner-sphere reorganization energy and show that the temperature dependence of the KIE is reproduced qualitatively for inner-sphere reorganization energies of 10−30 kcal/mol, but the temperature dependence of the rates increases as the inner-sphere reorganization energy increases mainly due to an increase in the free energy barrier.

We calculated the outer-sphere reorganization energies due to the protein with the FRCM method for conformations with C−O distances of 2.83, 3.0, and 3.2 Å. The calculated diabatic outer-sphere reorganization energies for PT ($1a \rightarrow 1b$), ET ($1a \rightarrow 2a$), and EPT ($1a \rightarrow 2b$) are 1.8, 3.8, and 2.4 kcal/mol, respectively, for the conformation with a C−O distance of 2.83 Å. The calculated diabatic solvent reorganization energy for EPT varied by less than 0.3 kcal/mol for the three different conformations, and therefore we concluded that the solvent reorganization energies are not sensitive to the specific choice of conformation. These outer-sphere reorganization energies are small compared to those calculated for analogous reactions in polar solvents because the dielectric constant for the protein is relatively small. Furthermore, the outer-sphere reorganization energy is smaller for EPT than for ET because the electron and proton are transferred in the same direction. The EPT reaction corresponds to a net hydrogen atom reaction, which involves a smaller change in the solute charge distribution than does the ET reaction.

**Classical Treatment of Donor−Acceptor Motion.** We calculated the rates and KIEs for the overall PCET reaction using the multistate continuum theory. The first step was to generate the two-dimensional free energy surfaces corresponding to the solvated reactant and product vibronic states as functions of the solvent coordinates $z_p$ and $z_e$ for a series of donor−acceptor distances $R$ along a grid. Using the parameters given in the previous section, we found that the equilibrium C−O distance and frequency are $R_I^o = 2.88$ Å and $\omega_I^o = 511$ cm$^{-1}$ at the minimum of the lowest energy reactant free energy surface. This frequency was calculated from the second derivative with respect to $R$ using a reduced mass of 6.86 g/mol corresponding to carbon and oxygen. Note that this frequency represents the local vibrational motion of the carbon and oxygen atoms and is not directly related to a "gating" frequency of the protein as discussed in ref 12. Nevertheless, the protein motion is expected to influence the local proton donor−acceptor vibrational motion.

As discussed above, five parameters were fit to five experimentally determined quantities. Specifically, the relative energies $\Delta E_{1b}$, $\Delta E_{2a}$, and $\Delta E_{2b}$ were fit to the experimentally determined reaction free energies in eq 14, and the couplings $V^{ET}$ and $V^{PT}$ were fit to the experimental rate and KIE at $T = 303$ K. No other parameters were adjusted. The temperature dependence of the rates was calculated from eq 8. (For simplicity, all input quantities were assumed to be independent of temperature.) The resulting temperature dependences of the hydrogen and deuterium rates, as well as the KIE, are depicted in Figure 5. This figure illustrates that the calculated rates and KIEs agree with the experimental data for these parameter values. As discussed
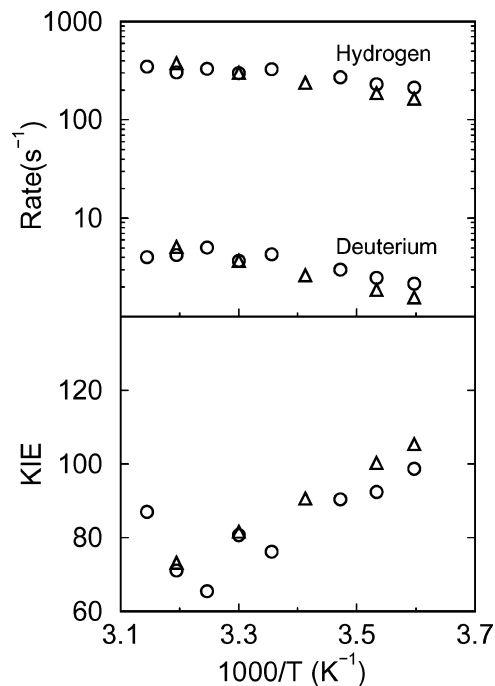


**Figure 5.** Temperature dependence of the rates and KIEs for multistate continuum theory calculations with a classical treatment of the proton donor−acceptor vibrational motion. The experimental data are denoted with circles, and the theoretical results are denoted with triangles. The calculations use the original parameter set. The equilibrium C−O distance and frequency are $R_I^o = 2.88$ Å and $\omega_I^o = 511$ cm$^{-1}$, and the dominant C−O distance is $R_{dom} = 2.69$ Å.
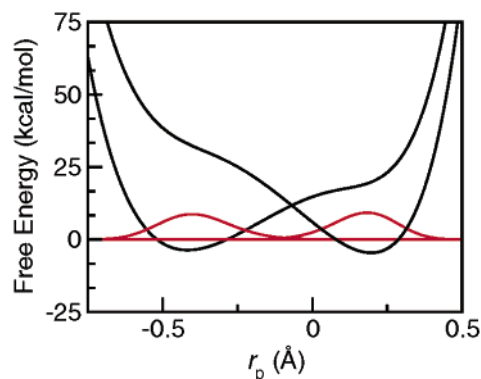


**Figure 6.** Reactant and product proton potential energy curves (black) and the associated proton vibrational wave functions (red) for the lowest energy reactant and product states at the lowest energy intersection point of the two-dimensional free energy surfaces for $R = 2.69$ Å. The overlap of these hydrogen vibrational wave functions is 0.0093, and the corresponding overlap of the deuterium vibrational wave functions is 0.00086.

below, this agreement with experimental data can be achieved for a range of physically reasonable parameter values.

We examined the origin of the unusually large KIE for this reaction. We found that the dominant contribution to the rate in eq 8 arises from the lowest energy reactant and product vibronic states. The hydrogen potential energy curves and the associated proton vibrational wave functions for these vibronic states are depicted in Figure 6. The relatively small overlap between these two wave functions leads to a large KIE. As discussed previously,[47] the KIE for each pair of states is approximately proportional to the square of the ratio of the

(47) Iordanova, N.; Hammes-Schiffer, S. *J. Am. Chem. Soc.* **2002**, *124*, 4848−4856.
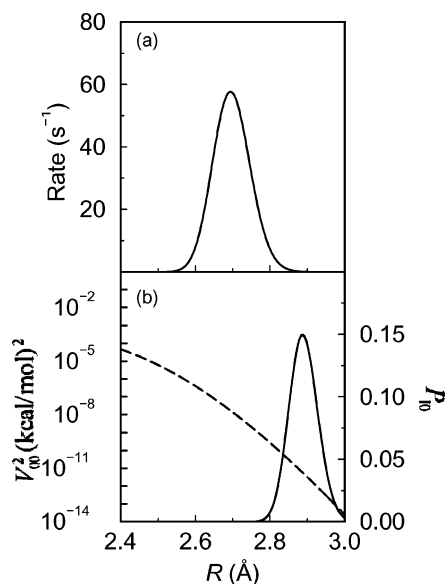
**Figure 7.** Analysis of the theoretical calculations with a classical treatment of the proton donor−acceptor vibrational motion. (a) Contribution to the overall rate as a function of the proton donor−acceptor distance $R$. The overall rate is obtained by integration of this function. The dominant contribution to the overall PCET rate corresponds to the distance $R_{dom} = 2.69$ Å. (b) The square of the coupling $V_{00}^2$ (dashed) and the Boltzmann probability $P_{I0}$ (solid) for the lowest energy reactant and product states as functions of the proton donor−acceptor distance $R$. The equilibrium donor−acceptor distance on the lowest energy reactant free energy surface is $R_I^o = 2.88$ Å.
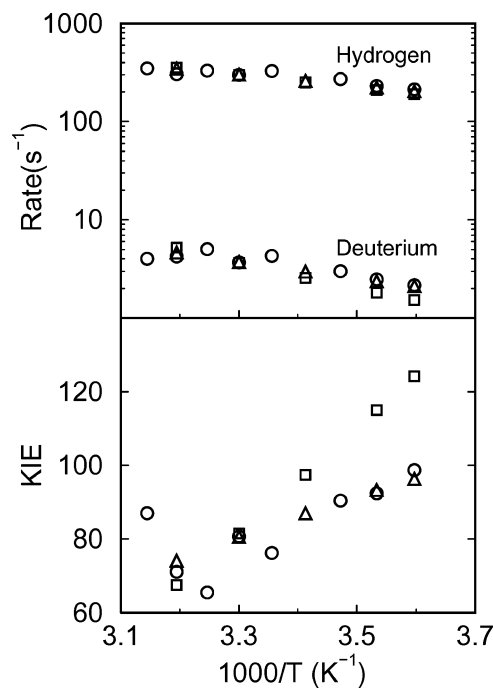


**Figure 8.** Temperature dependence of the rates and KIEs for multistate continuum theory calculations with a fixed proton donor−acceptor distance. The experimental data are denoted with circles. The theoretical results were generated with fixed proton donor−acceptor distances of $R = 2.7$ Å (triangles) and 2.8 Å (squares).

overlap for hydrogen to the overlap for deuterium. This ratio increases as the vibrational wave function overlap decreases. Moreover, since the vibrational overlap is smallest for the reactive channel involving the lowest energy reactant and product vibronic states, the overall KIE decreases as the contributions from channels involving higher energy vibronic states increase. Thus, the unusually large KIE for lipoxygenase is due to the relatively small overlap of the vibrational wave functions and the dominance of the lowest energy reactant and product vibronic states in the tunneling process.

We investigated the importance of the proton donor−acceptor vibrational motion to the PCET rate. As mentioned above, the equilibrium proton donor−acceptor distance is $R_I^o = 2.88$ Å for the lowest energy reactant free energy surface. In contrast, the dominant contribution to the overall PCET rate (eq 8) at $T = 303$ K arises from a proton donor−acceptor distance of $R_{dom} = 2.69$ Å, as illustrated in Figure 7a. The dominant proton donor−acceptor distance is ∼0.02 Å smaller for deuterium than for hydrogen and varies by ∼0.02 Å over the temperature range studied. Figure 7a indicates that the contribution from the equilibrium donor−acceptor distance of $R_I^o = 2.88$ Å to the overall PCET rate is negligible. We analyzed the various terms in the rate expression to understand the origin of this phenomenon. The reaction free energies and the reorganization energies do not depend strongly on the proton donor−acceptor distance. As illustrated in Figure 7b, the coupling $V_{\mu\nu}$ given in eq 7 increases significantly as the proton donor−acceptor distance decreases. This increase in the coupling is due mainly to the increase in the overlap between the reactant and product proton vibrational wave functions as $R$ decreases. On the other hand, the Boltzmann probability $P_{I\mu}(R)$ has a maximum at $R \approx 2.88$ Å, as depicted in Figure 7b. The dominant proton donor−

acceptor distance for the overall PCET reaction is determined by a balance between the larger coupling and the smaller Boltzmann probability as the distance decreases.

**Fixed Donor−Acceptor Distance.** To further analyze the role of the proton donor−acceptor vibrational mode, we calculated the rates and KIEs for fixed donor−acceptor distances of $R = 2.7$ and 2.8 Å using eq 2. As for the previous calculations, the relative energies of the four diabatic states were fit to the experimentally determined reaction free energies in eq 14, and the couplings $V^{ET}$ and $V^{PT}$ were fit to the experimental rate and KIE, respectively, at $T = 303$ K, but no other parameters were adjusted. Figure 8 illustrates that the experimental temperature dependence of the rates and KIEs can be reproduced for the fixed proton donor−acceptor distance of $R = 2.7$ Å. Note that this donor−acceptor distance is similar to the distance corresponding to the dominant contribution to the overall PCET rate calculated with eq 8 but is considerably smaller than the equilibrium donor−acceptor distance for this model.

Figure 8 also illustrates that the experimental temperature dependence of the KIEs is not reproduced for the fixed proton donor−acceptor distance $R = 2.8$ Å. Specifically, the slope of the KIE as a function of $1/T$ is much larger for $R = 2.8$ Å. For shorter proton donor−acceptor distances, the temperature dependence of the KIE is weaker than the experimentally observed temperature dependence. For the fixed proton donor−acceptor distance of $R = 2.6$ Å, we were unable to reproduce the high KIE of 81 at $T = 303$ K due to the large overlap between the reactant and product hydrogen vibrational wave functions at this shorter distance. Analysis of the terms in the rate expression indicates that at larger proton donor−acceptor distances, the excited vibronic states contribute more significantly to the overall rate. In general, the relative contributions

of the vibronic states are determined by a competition between the coupling, which favors the higher states, and the free energy barrier, which favors the lower states in the normal Marcus region. As the proton donor−acceptor distance increases, the coupling for the lowest energy reactant and product states decreases due to the averaging over the reactant and product vibrational wave functions, thereby leading to greater contributions from the excited vibronic states. Moreover, the relative contributions of the excited states are different for hydrogen and deuterium and depend strongly on the temperature. This analysis suggests that the proton donor−acceptor vibrational motion plays a vital role in decreasing the dominant proton donor−acceptor distance relative to its equilibrium value to facilitate the reaction.

**Quantum Treatment of Donor−Acceptor Motion.** We have also performed multistate continuum theory calculations in which the donor−acceptor vibrational motion is treated quantum mechanically.[26] In this case, the vibrational wave functions depend on the hydrogen coordinate $r$ and the proton donor−acceptor distance $R$, and the rate expression has the same general form as eq 2. The results obtained with the quantum treatment of the donor−acceptor mode for two different parameter sets are provided in Supporting Information. For the original parameter set used to generate Figure 5 with the classical treatment of the donor−acceptor mode, the quantum treatment slightly overestimates the rates and underestimates the KIEs, but the temperature dependence of the rates and KIE agree well with the experimental data and the classical treatment of the donor−acceptor mode. When the couplings $V^{ET}$ and $V^{PT}$ were adjusted slightly ($V^{ET} = 0.022$ kcal/mol and $V^{PT} = 18.25$ kcal/mol) to fit the experimental rate and KIE at $T = 303$ K, the results obtained with the quantum treatment of the donor−acceptor mode agree well with the experimental data.

**Parameter Dependence.** We investigated the dependence of the results on the reorganization energies. As mentioned above, the outer-sphere reorganization energy was calculated with the FRCM method for several different conformations corresponding to proton donor−acceptor distances of $R = 2.8$−$3.2$ Å. The diabatic outer-sphere reorganization energies for EPT were found to be the same to within 0.3 kcal/mol for these different conformations. The calculation of the inner-sphere reorganization energy of 19.1 kcal/mol is not straightforward because it is based on relatively small changes in bond lengths for DFT calculations and neglects the inner-sphere reorganization energy of the linoleic acid. The rates and KIEs for inner-sphere reorganization energies of $\lambda_{in} = 10$ kcal/mol and $\lambda_{in} = 30$ kcal/mol are provided in Supporting Information. The temperature dependence of the KIE is reproduced reasonably well for inner-sphere reorganization energies in the range $\lambda_{in} = 10$−$30$ kcal/mol, although the slope increases slightly as the inner-sphere reorganization energy increases. The magnitude of the slope of the temperature dependence of the rates increases as the inner-sphere reorganization energy increases mainly due to an increase in the free energy barrier.

We also investigated the dependence of the results on the gas-phase EVB potential parameters. The C−H and O−H Morse parameters are determined by experimentally determined frequencies, bond lengths, and dissociation energies. Variation of these parameters within the physically reasonable range does not significantly influence the results. On the other hand, the

results are sensitive to the C−O equilibrium distances and frequencies on the free energy surfaces representing the reactant and product vibronic states. These properties of the free energy surfaces are determined mainly by the Fe−O and $\pi$−C force constants and the C−O Morse parameters. We emphasize that the C−O equilibrium distances and frequencies on the free energy surfaces are not determined solely by the C−O Morse parameters but rather are strongly influenced by the other terms in the EVB potential such as the Fe−O and $\pi$−C frequencies. We performed a detailed analysis based on systematic variation of these parameters.

For the first model studied, the Fe−O and $\pi$−C force constants were chosen to correspond to physically reasonable frequencies for those types of modes. For these parameter values, the results were relatively insensitive to the choice of the C−O Morse parameter $\beta_{CO}$ because the Fe−O and $\pi$−C force constants dominated the overall C−O frequency. The temperature dependence of the rates and KIEs are reproduced for $\beta_{CO} = 1.21$−$3.62$ Å$^{-1}$, which corresponds to C−O Morse frequencies of 200−600 cm$^{-1}$ and C−O frequencies on the free energy surfaces of $\omega_I^o = 460$−$580$ cm$^{-1}$. Although the results are relatively insensitive to $\beta_{CO}$ for these Fe−O and $\pi$−C force constants, the results are very sensitive to the value of the C−O Morse parameter $R_{CO}^o$, which influences the equilibrium C−O distance. The results for $R_{CO}^o = 3.0$ Å, which corresponds to an equilibrium C−O distance on the free energy surface of $R_I^o = 3.05$ Å, are provided in Supporting Information. In this case, the slope of the temperature dependence of the KIE is too large, and the dominant proton donor−acceptor distance contributing to the rate is $R_{dom} = 2.79$ Å, which is significantly larger than the dominant distance of $R_{dom} = 2.69$ Å for the original parameter set. We found that the slope of the temperature dependence of the KIE increases as the dominant proton donor−acceptor distance increases, because the contributions of the excited vibronic states increase for larger distances. The physical basis for this observation is described above in the discussion of the calculations with fixed proton donor−acceptor distances.

**Alternative Model.** We have also developed an alternative model that allows larger equilibrium C−O distances. As discussed above, the equilibrium C−O distance and frequency are $R_I^o = 2.88$ Å and $\omega_I^o = 511$ cm$^{-1}$ in the first model studied. This equilibrium C−O distance of $R_I^o = 2.88$ Å is significantly smaller than the sum of the corresponding van der Waals radii of ~3.2 Å. In the alternative model, the harmonic terms $U_{FeO}^{harm}$ and $U_{\pi C}^{harm}$ are chosen to be relatively small and are not associated with any physical properties. In this case, the equilibrium C−O frequency on the free energy surface is determined mainly by the frequency associated with the C−O Morse potential (i.e., the parameter $\beta_{CO}$) and represents an effective frequency resulting from motions of the substrate, protein, and iron complex. We found that the equilibrium C−O frequency must be decreased significantly to fit the data for larger equilibrium C−O distances. The outer-sphere reorganization energies were calculated for a conformation with a C−O distance of 3.0 Å. The couplings $V^{ET}$ and $V^{PT}$ were fit to the experimental rate and KIE, respectively, at $T = 303$ K. The results obtained with this alternative model are provided in Supporting Information. For this model, the equilibrium C−O distance and frequency are $R_I^o = 3.05$ Å and $\omega_I^o = 284$ cm$^{-1}$, respectively, on the lowest energy reactant free energy surface.

The dominant proton donor−acceptor distance contributing to the rate is $R_{dom} = 2.69$ Å, which is identical to the dominant distance for the smaller equilibrium C−O distance of $R_I^o = 2.9$ Å. These results indicate that the temperature dependence of the KIE can be reproduced by larger equilibrium C−O distances if the C−O frequency is low enough to allow the dominant distance contributing to the rate to be $R_{dom} \approx 2.7$ Å. As discussed above, the dominant distance is determined by a balance between the coupling and the Boltzmann probability.

**Comparison to Previous Calculations.** Previously, Klinman and co-workers[12] applied a simpler tunneling theory to this reaction. This previous application used an equation[48] based on Marcus theory for ET with only two electronic states, rather than the four diabatic electronic states used in the multistate continuum theory for PCET. In the two-state formulation,[22,23] the reorganization energies and reaction free energies are assumed to be the same for all pairs of vibronic states, and the electronic coupling is separable from the proton vibrational wave functions. In the four-state formulation,[17,18] the reorganization energies and reaction free energies differ for each pair of vibronic states because of variations in the relative weights of the PT diabatic states, and the electronic coupling is not rigorously separable from the proton vibrational wave functions because it depends on the proton coordinate.

The present approach differs from Klinman and co-workers' approach in the treatment of the proton coordinate. In Klinman and co-workers' approach,[12] the proton potential is assumed to be harmonic with the same frequency for both the reactant and product. Thus, the overlap reduces to an integral over harmonic oscillator wave functions, and the energies of the proton vibrational states are assumed to be equally spaced. This previous approach neglects changes in the shape of the proton potential (i.e., the tunneling barrier) due to the proton donor−acceptor vibrational motion. In the present approach, however, each diabatic state includes a Morse potential for the donor-hydrogen or acceptor-hydrogen motion, and the overall potential energy surface is a mixture of these diabatic states. Thus, the potential energy surface includes the anharmonicity of the hydrogen motion and provides a physically reasonable description of the dependence of the barrier on the proton donor−acceptor distance. Moreover, in the present formulation the coupling is calculated by numerical integration of eq 7 and includes the dependence of the electronic coupling on the proton coordinate as well as the anharmonic effects in the vibrational wave functions. The reorganization energies and reaction free energies are calculated numerically for each vibronic state without the assumption of equal spacing for the energies of the hydrogen vibrational states.

The present approach also differs significantly from Klinman and co-workers' approach in the treatment of the proton donor−acceptor mode, which is denoted the "gating" coordinate in ref 12. In Klinman and co-workers' approach,[12] only the Franck−Condon overlap term depends on the gating coordinate, and the motion of the gating coordinate is assumed to be harmonic. In the present formulation, the overall free energy surfaces depend on the proton donor−acceptor distance because diagonal and off-diagonal gas-phase valence bond matrix elements depend on the donor−acceptor coordinate. Thus, the reorganization energies, reaction free energies, and couplings in the rate

(48) Kuznetsov, A. M.; Ulstrup, J. *Can. J. Chem.* **1999**, *77*, 1085−1096.

expression depend on the proton donor−acceptor distance. Moreover, the anharmonicity of the donor−acceptor motion is included by using a Morse potential to describe the proton donor−acceptor motion in the diabatic states. In addition, Klinman and co-workers treated the gating mode classically, whereas we performed calculations with both classical and quantum treatments of the proton donor−acceptor mode.

The parametrization of the potential energy term describing the donor−acceptor motion also differs for the two approaches. Klinman and co-workers[12] represent the gating mode with a mass of 110 g/mol, corresponding to the mass of an amino acid, and a frequency of 400 cm$^{-1}$. The present calculations represent the donor−acceptor mode with a mass of 6.86 g/mol, corresponding to the reduced mass of carbon and oxygen, and a frequency of 300−500 cm$^{-1}$. The force constant used in Klinman and co-workers' calculations is more than a factor of 10 larger than the effective force constant based on the second derivative of the free energy surface with respect to the donor−acceptor distance used in the present calculations. Thus, the motion is much stiffer for the gating mode in Klinman's calculations than for the donor−acceptor mode in the present calculations. As a result of this stiffer motion of the gating mode, the equilibrium tunneling distance (defined in ref 12 as the separation between the minima of the donor and acceptor wells along the hydrogen coordinate) is required to be smaller in Klinman and co-workers' calculations than in the present calculations. Klinman and co-workers' calculations required a donor−acceptor distance of 2.8 Å, whereas we are able to reproduce the experimental temperature dependence with an equilibrium donor−acceptor distance of 3.1 Å in conjunction with an equilibrium donor−acceptor frequency of 300 cm$^{-1}$. Moreover, the equilibrium donor−acceptor distance can be increased further if the frequency is decreased within the framework of our theoretical formulation.

Many of the conclusions in the present article are similar to those of Klinman and co-workers.[12] To fit the experimental kinetic data, Klinman and co-workers used a total reorganization energy of 19.5 kcal/mol, which is similar to our calculated value of 21.0 kcal/mol for the lowest energy reactant and product PCET states. Note that we calculated the inner-sphere and outer-sphere reorganization energies independently with quantum mechanical methods. Klinman and co-workers were also able to fit the temperature dependence of the KIE without inclusion of the proton donor−acceptor vibrational motion if they used a shorter hydrogen transfer distance.

Several central conclusions from the work of Klinman and co-workers[12] differ substantially from the conclusions of the present work. Klinman and co-workers conclude that the rates and KIEs will become more temperature-dependent as the gating frequency decreases because a larger range of donor−acceptor distances will be thermally accessible for lower frequencies. According to ref 12, decreasing the frequency of the gating mode increases the temperature dependence of the tunneling distance, which is different for hydrogen and deuterium, leading to a greater temperature dependence of the KIE. Their model indicates that an extremely stiff gating frequency is required to reproduce the experimental data for wild-type SLO (i.e., gating does not significantly modulate the hydrogen transfer distance). Thus, they conclude that the active site for wild-type SLO is highly preorganized with a relatively short proton donor−

acceptor distance. In the present work, the temperature dependence of the KIE is found to be strongly influenced by the donor–acceptor distance with the dominant contribution to the overall rate. The KIE becomes more temperature dependent as this dominant distance increases because excited vibronic states play a greater role at larger distances. (This phenomenon is discussed above in the context of calculations with fixed proton donor–acceptor distances.) The relative contributions of these excited states depend strongly on temperature and vary for hydrogen and deuterium. Within the framework of our theoretical formulation, the dominant distance depends on the equilibrium donor–acceptor distance and frequency. For a physically reasonable equilibrium donor–acceptor distance, the temperature dependence of the KIE increases as the frequency increases because the dominant donor–acceptor distance increases (i.e., smaller donor–acceptor distances are not thermally accessible). We are able to reproduce the experimental data for wild-type SLO with a larger equilibrium donor–acceptor distance by decreasing the corresponding frequency. We conclude that the relatively low-frequency donor–acceptor vibrational motion is critical in SLO to decrease the donor–acceptor distance from its equilibrium value to allow hydrogen tunneling.

Solomon and Lehnert also used computational methods to study this reaction.[11] As mentioned above, their density functional theory calculations indicate that the reaction occurs through a PCET mechanism in which the electron transfers from the $\pi$-system of the substrate to the iron as the proton transfers from the carbon to the oxygen. This conclusion is consistent with the thermodynamic analysis presented in the Appendix. Solomon and Lehnert also observed that the calculated energy barriers for this process depend strongly on the proton donor–acceptor distance. The calculated barrier for hydrogen transfer is 30 kcal/mol at the stated crystallographic donor–acceptor distance of 3.0 Å, but protein fluctuations are expected to decrease the distance and thereby lower the barrier. Solomon and Lehnert hypothesize that the hydrogen transfer reaction in SLO occurs at a donor–acceptor distance of ∼2.7 Å with a barrier of 15 kcal/mol including zero-point energy corrections. A simple hydrogen tunneling model is used to explain the small activation energy that was observed experimentally. The hydrogen transfer donor–acceptor distance proposed by Solomon and Lehnert[11] is consistent with the results of the present work.

## V. Conclusions

In this article, we applied a multistate continuum theory to the PCET reaction catalyzed by the enzyme SLO. The inner-sphere reorganization energy of the iron cofactor for the PCET reaction was estimated to be ∼19 kcal/mol based on DFT B3LYP calculations on a model system. The diabatic outer-sphere reorganization energy of the protein for EPT was calculated to be 2.4 kcal/mol with the frequency-resolved cavity model for a conformation obtained from docking simulations. These calculations indicate that the inner-sphere reorganization energy is significantly larger than the outer-sphere reorganization energy of the protein for this process. The free energy of reaction for PCET was estimated to be −5.4 kcal/mol from experimentally determined thermodynamic properties. In contrast, the free energies of reaction for ET and PT were estimated to be substantially endothermic. This thermodynamic analysis implies that the electron and proton transfer simultaneously rather than sequentially. The reorganization energies and estimated reaction

free energies were used in conjunction with the multistate continuum theory to calculate the rates and KIEs for the PCET reaction.

The temperature dependence of the calculated rates and KIEs is in agreement with the experimental data. A detailed analysis of the terms in the PCET rate expression provides further insight into the mechanism. The lowest energy reactant and product vibronic states were found to represent the dominant contribution to the overall rate. The weak temperature dependence of the rates is due to a relatively small free energy barrier, which derives from a balance between the total reorganization energy and the reaction free energy. The temperature dependence of the rates was found to increase for larger values of the inner-sphere reorganization energy mainly due to an increase in the free energy barrier. The unusually high KIE of 81 results from the small overlap of the reactant and product proton vibrational wave functions and the dominance of the lowest energy reactant and product vibronic states in the hydrogen tunneling process.

We also investigated the role of the proton donor–acceptor vibrational motion in this PCET reaction. The effects of the proton donor–acceptor vibrational motion were examined with both a classical treatment involving thermal averaging over the donor–acceptor distances and a quantum mechanical treatment of the donor–acceptor mode. The results obtained from the classical and quantum treatments were qualitatively similar. Thus, the quantum mechanical effects associated with the donor–acceptor mode are not critical for the description of the temperature dependence of the rates and KIEs within the relevant temperature range. For the classical treatment, the dominant contribution to the overall PCET rate was found to correspond to a proton donor–acceptor distance that is considerably smaller than the equilibrium donor–acceptor distance in this model. Analysis of the results indicates that the dominant proton donor–acceptor distance is determined by a balance between the larger coupling and the smaller Boltzmann probability as the distance decreases. Although the dominant proton donor–acceptor distance is energetically unfavorable relative to the equilibrium distance, this dominant distance is sampled through thermal fluctuations and contributes significantly to the overall rate due to the large coupling.

For comparison, we also performed calculations for fixed proton donor–acceptor distances. We found that the temperature dependence of the rates and KIEs could be reproduced with a fixed proton donor–acceptor distance that is similar to the dominant distance in the calculations including the proton donor–acceptor vibrational motion. On the other hand, we were unable to reproduce the temperature dependence of the KIEs with the larger equilibrium proton donor–acceptor distance for this model. Our analysis indicates that the experimental temperature dependence cannot be reproduced with the proton donor–acceptor distance fixed at its equilibrium value due to the increased contributions of the excited vibronic states for the larger donor–acceptor distances. The relative contributions of these excited states are different for hydrogen and deuterium and vary significantly with temperature.

Thus, this study illustrates that the proton donor–acceptor vibrational motion plays a vital role in decreasing the dominant donor–acceptor distance relative to its equilibrium value to facilitate the PCET reaction. We reproduced the experimentally determined temperature dependence of the rates and KIEs with

two different models. In the first model, the equilibrium C−O distance and frequency are 2.9 Å and 500 cm$^{-1}$, respectively. In the second model, the equilibrium C−O distance and frequency are 3.1 Å and 300 cm$^{-1}$, respectively. For both models, the proton donor−acceptor distance with the dominant contribution to the overall rate is 2.7 Å. For the range of temperatures studied, the temperature dependence of the KIE is determined largely by this dominant donor−acceptor distance. The dominant distance is determined by numerous factors, including the equilibrium donor−acceptor distance and frequency. Within the framework of this theoretical formulation, the frequency of the donor−acceptor vibrational mode must be decreased as the equilibrium donor−acceptor distance is increased to maintain the same dominant donor−acceptor distance for the overall rate.

These calculations lead to several general predictions concerning the rates and KIEs of PCET reactions in enzymes. The temperature dependence of the rates is determined mainly by the free energy barrier, which depends on the reorganization energy and the reaction free energy. The magnitude of the KIE increases as the overlap between the reactant and product hydrogen vibrational wave functions decreases and the contributions of excited vibronic states decrease. As the proton donor−acceptor distance increases, typically the overlap between the reactant and product hydrogen vibrational wave functions decreases and the contributions of excited vibronic states increase. Thus, if all other factors remain constant, this theory predicts that the temperature dependence of the KIE will increase as the dominant donor−acceptor distance increases. In general, however, the magnitude of the KIE is determined by a complex balance of numerous factors, including the dominant proton donor−acceptor distance, the reorganization energy, the reaction free energy, and the electronic couplings. Similarly, the temperature dependence of the KIE is strongly influenced by the dominant proton donor−acceptor distance but also depends on other factors such as the reorganization energy, reaction free energy, and electronic couplings.

Although these model calculations provide insight into the fundamental principles of the PCET reaction catalyzed by SLO, a number of important issues remain unresolved. The detailed mechanism by which the protein environment facilitates the PCET reaction is not well understood. Moreover, the role of dynamical effects in this reaction has not been investigated. Hybrid quantum/classical molecular dynamics simulations including the explicit protein can be used to address these issues. In addition, these types of simulations may be used to elucidate the impact of enzyme mutations on the overall reaction.

## Appendix

This appendix outlines the method for estimating the experimentally determined driving forces (i.e., reaction free energies) for ET, PT, and PCET. Note that the substantial uncertainties in these estimated driving forces do not alter the qualitative results in this article.

**Electron Transfer.** The electron transfer reaction from linoleic acid to the iron complex is

$$CH + HO-Fe(III) \rightarrow CH^+ + HO-Fe(II) \quad (A1)$$

Equation A1 is the sum of eqs A2 and A3:

$$CH \rightarrow CH^+ + e^- \quad (A2)$$

$$HO-Fe(III) + e^- \rightarrow HO-Fe(II) \quad (A3)$$

The reduction potential for eq A2 is $E° = 2.7$ V (vs NHE) for arachidonic acid in acetonitrile.[49] We estimate that the potential will be lower in water by approximately 0.4 V,[50] leading to $E° = 2.3$ V (vs NHE) in water. Equation A3 is the sum of eqs A4 and A5:
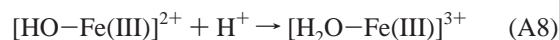
$$HO-Fe(III) + e^- + H^+ \rightarrow H_2O-Fe(II) \quad (A4)$$

$$H_2O-Fe(II) \rightarrow HO-Fe(II) + H^+ \quad (A5)$$
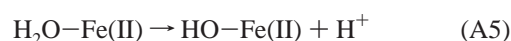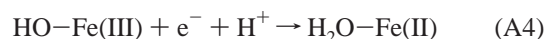
The reduction potential for eq A4 in SLO1 is $E° = 0.6$ V at pH $= 8,$[51] leading to $E° = 0.6 + 0.059(8)$ V $= 1.1$ V at pH $= 0$. The $pK_a$ for $H_2O-Fe(II)$ in SLO1 has been determined to be $\geq 11.5.$[2] Using a $pK_a$ of 11.5, $\Delta G° = 1.368$ $pK_a$ kcal/mol $= 15.73$ kcal/mol. Therefore, the overall free energy of the reaction in eq A1 is estimated to be $\Delta G° = [-23.061(-2.3 + 1.1) + 15.73]$ kcal/mol $= 43$ kcal/mol.

**Proton Transfer.** The proton transfer reaction from linoleic acid to the hydroxide ligand on iron in SLO1 is

$$CH + [HO-Fe(III)]^{2+} \rightarrow C^- + [H_2O-Fe(III)]^{3+} \quad (A6)$$
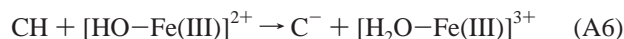
Equation A6 is the sum of eqs A7 and A8:

$$CH \rightarrow C^- + H^+ \quad (A7)$$

$$[HO-Fe(III)]^{2+} + H^+ \rightarrow [H_2O-Fe(III)]^{3+} \quad (A8)$$

The free energy of the reaction in eq A7 for 1,4-pentadiene in DMSO is estimated to be 43 kcal/mol (where the enthalpy was measured to be 40 kcal/mol and the entropy contribution is approximated as 3 kcal/mol).[52] Estimating a decrease in the $pK_a$ of ∼3 units in water relative to DMSO,[53−55] the free energy of the reaction in eq A7 for linoleic acid in water is estimated to be $\Delta G° = 39$ kcal/mol. The $pK_a$ for $H_2O-Fe(III)$ in SLO1 has been determined to be <6.[56] Using a $pK_a$ of 5, $\Delta G° = -1.368$ $pK_a$ kcal/mol $= -6.84$ kcal/mol for the reaction in eq A8. Therefore, the overall free energy of the reaction in eq A6 is estimated to be $\Delta G° = [39 - 6.84]$ kcal/mol $= 32$ kcal/mol.

**PCET.** The PCET reaction from linoleic acid to the iron complex in SLO1 is

$$CH + HO-Fe(III) \rightarrow C^\bullet + Fe(II)-OH_2 \quad (A9)$$

(49) Wiseman, J. S. *Biochemistry* **1989**, *28*, 2106−2111.
(50) Parker, V. D. *J. Am. Chem. Soc.* **1992**, *114*, 7458−7462.
(51) Nelson, M. J. *Biochemistry* **1988**, *27*, 4273−4278.
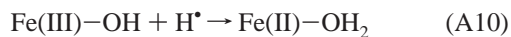(52) Arnett, E. M.; Venkatasubramaniam, K. G. *J. Org. Chem.* **1983**, *48*, 1569−1574.
(53) Bordwell, F. G. *Acc. Chem. Res.* **1988**, *21*, 456−463.
(54) Wayner, D. D. M.; Parker, V. D. *Acc. Chem. Res.* **1993**, *26*, 287−294.
(55) Bordwell, F. G. *Pure Appl. Chem.* **1977**, *49*, 963−968.
(56) Scarrow, R. C.; Trimitsis, M. G.; Buck, C. P.; Grove, G. N.; Cowling, R. A.; Nelson, M. J. *Biochemistry* **1994**, *33*, 15023−15035.

Equation A9 is the sum of eqs A10 and A11:

$$\text{Fe(III)}-\text{OH} + \text{H}^\bullet \rightarrow \text{Fe(II)}-\text{OH}_2 \quad (A10)$$

$$\text{CH} \rightarrow \text{C}^\bullet(\text{aq}) + \text{H}^\bullet \quad (A11)$$

On the basis of the reduction potential[51] of eq A4 and the conversion to an aqueous bond enthalpy,[57] the free energy change associated with eq A10 is estimated to be $\Delta G° = -82$ kcal/mol.[12] The bond strength of 1,4-pentadiene is 76.6 kcal/mol,[58] and assuming negligible entropy change upon reaction,

---

(57) Mayer, J. M. *Acc. Chem. Res.* **1998**, *31*, 441−450.

$\Delta G° = 76.6$ kcal/mol for the reaction in eq A11. Therefore, the overall free energy of the reaction in eq A9 is estimated to be $\Delta G° = [-82 + 76.6]$ kcal/mol = $-5.4$ kcal/mol.

**Supporting Information Available:** Four figures depicting the temperature dependence of the rates and KIEs are provided to illustrate the parameter dependence of these results, and a table with the Ahrrenius activation energies for the various models is also provided (PDF). This material is available free of charge via the Internet at http://pubs.acs.org.

---

(58) Clark, K. B.; Culshaw, P. N.; Griller, D.; Lossing, F. P.; Simoes, J. A. M.; Walton, J. C. *J. Org. Chem.* **1991**, *56*, 5535−5539.